Chemical Geology 604 (2022) 120948

Contents lists available at ScienceDirect

Chemical Geology

journal homepage: www.elsevier.com/locate/chemgeo

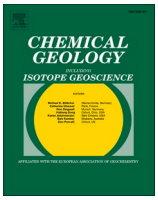

Distribution patterns of dissolved trace metals (Fe, Ni, Cu, Zn, Cd, and Pb) in China marginal seas during the GEOTRACES GP06-CN cruise

Ruifeng Zhang [a,*], Jingling Ren [b], Zhaoru Zhang [a], Zhu Zhu [a], Seth John [c]

[a] School of Oceanography, Shanghai Jiao Tong University, Shanghai, China
[b] Frontiers Science Center for Deep Ocean Multispheres and Earth System, and Key Laboratory of Marine Chemistry Theory and Technology, Ministry of Education, Ocean University of China, Qingdao 266100, China
[c] Department of Earth Sciences, University of Southern California, Los Angeles, CA, United States

ARTICLE INFO

Editor: Karen Johannesson

Keywords:
Trace metals
Marginal seas
GEOTRACES
Tracer

ABSTRACT

Trace metals are both important micronutrients for life in the oceans, and can be tracers of various natural and anthropogenic processes. Metals including Fe, Ni, Zn, and Cu are known to be important nutrients for phytoplankton, elements including Pb are viewed primarily as anthropogenic contaminants, Cd is a biologically cycled element though it's nutritive importance is unclear, and all of these metals are impacted by overlapping natural and anthropogenic processes in different parts of the oceans. China is bordered by four marginal seas, including the Bohai, Yellow Sea (YS), East China Sea (ECS), and South China Sea. Here we present the first systematic study of trace metals in the China marginal seas from the GEOTRACES GP06CN cruise in October 2015. The metals Fe, Ni, Cu, Zn, Cd, and Pb were sampled in the Yellow Sea and East China Sea at 69 surface locations using a towfish and with 8 depth profiles, along with auxiliary parameters including salinity, phosphate, and apparent oxygen utilization. We find that Ni, Cu and Cd are most strongly impacted by a combination of biological cycling and fluvial inputs, recent atmospheric deposition dominates surface ocean Pb concentrations, and Fe and Zn are impacted by a combination of multiple processes. Comparison with historical data shows that Cu concentrations have been increasing through time, presumably due to increasing anthropogenic inputs. Ni and Cd are also delivered in high concentrations from rivers, which can reflect the impact of anthropogenic inputs, and Pb is delivered from atmospheric deposition which may include anthropogenic sources, but these metals do not show a distinct temporal trend. The six metals studied here are thus impacted by their broad-scale oceanographic distributions, local coastal processes, and anthropogenic inputs, each in different ways and to different degrees. This study represents a unique contribution to the international GEOTRACES effort, by highlighting an 'end-member' region with strong coastal and anthropogenic inputs.

1. Introduction

The biogeochemical cycles of trace metals in the ocean are important due to the role they play in marine life and thus their influence on the global carbon cycle and climate. Iron (Fe) is perhaps the best example of this, contributing to many essential metabolic processes, and limiting primary production in a vast ocean area where macronutrient concentrations in the surface are high (Boyd et al., 2007; Martin, 1990). Other metals are also biologically important, for example nickel (Ni) is identified as a co-factor in urease and superoxide dismutase (Cuvelier et al., 2010; Price and Morel, 1991), marine phytoplankton use zinc (Zn) and cadmium (Cd) as metal centers in carbonic anhydrase (Morel and Price, 2003), and copper (Cu) may replace Fe in certain biochemical functions in diatoms (Sunda and Huntsman, 1995). However, trace metals can be toxic to marine biota when their concentrations are too high in seawater, perhaps as a result of the nonfunctional substitution for essential metals (Sunda, 1989). Typically, vertical profiles of these dissolved trace metals exhibit nutrient-like patterns, with uptake by phytoplankton at the surface, and they are typically remineralized in close stoichiometry with macronutrients in the deeper water column (Bruland, 1980). Unlike the trace metals mentioned above, lead (Pb) is considered to have no positive biological utility in marine life. Pb has been identified as an

Abbreviations: CDW, Changjiang Diluted Water; ECS, East China Sea; ECSCC, East China Sea Coastal Current; KC, Kuroshio current; LBCC, Lubei Coastal Current; TWC, Taiwan Warm Current; YS, Yellow Sea; YECS, Yellow and East China Sea; YSCC, Yellow Sea Coastal Current.

* Corresponding author.
E-mail address: ruifengzhang@sjtu.edu.cn (R. Zhang).

https://doi.org/10.1016/j.chemgeo.2022.120948
Received 2 January 2022; Received in revised form 28 April 2022; Accepted 25 May 2022
Available online 29 May 2022

excellent tracer for anthropogenic sources of dust and particles to surface waters, owing to the anthropogenic emission over the past two centuries (Boyle et al., 2014).

Distribution of trace metals in seawater is determined by both their internal cycling in the water column and the interaction of their sources and sinks with other spheres. Key external sources of metals to the ocean include atmospheric deposition, sedimentary input, hydrothermal venting, and riverine input (Anderson, 2019). Marginal seas are located at the interface between land and open ocean, where the continental sources consist of both natural and anthropogenic metals, linking them both to local anthropogenic effects and to global biogeochemical cycles and climate (Chen et al., 2004; Siefert, 2004). Marginal seas play an important role as conduits passing metals from land to the ocean. Examples include the lateral transport of external Fe from marginal seas into the ocean basins (Jensen et al., 2020; Nishioka and Obata, 2017), cross-shelf transport of terrestrial Al along the isopycnal surface to the open ocean (Ren et al., 2015), and the transport of metals from riverine sources along the transpolar drift into the North Pole (Charette et al., 2020). Quantifying sources and sink of trace metals in marginal seas is therefore essential to elucidating trace metal biogeochemical cycling in the global oceans.

During the past three decades, China has experienced rapid industrialization and urbanization. China's coastline supports half of China's human population, leading to increasing anthropogenic stress on China marginal seas (He et al., 2014). Consequently, trace metal biogeochemical cycling in marginal seas may vary over time, along with changes in the flux of trace metals from various sources including rivers, atmospheric deposition, and groundwater, with the potential to impact ecosystems (Guo et al., 2014; Wang et al., 2013). However, the lack of trace metal sampling has limited the acquisition of information on trace metal distributions in the coastal waters of China seas. During the China-French and China-US joint studies conducted in the 1980s, researchers investigated trace metal behavior in several large Chinese river estuaries (Edmond et al., 1985; Elbaz-Poulichet et al., 1987; Zhang, 1995). Several subsequent studies have also studied the distribution of trace metals in the China marginal seas, for example, Cu in the Yellow Sea (YS) and East China Sea (ECS) (Abe et al., 2003), dissolved and particulate trace metals in the Changjiang Estuary (Jiann et al., 2009; Koshikawa et al., 2007; Zhu et al., 2018), Pb in the ECS (Jiang et al., 2018), and concentrations of several dissolved trace metals in the Bohai Sea and the YS (Li et al., 2015; Li et al., 2017). Yet, a comprehensive survey of multiple trace metals, in the style of recent GEOTRACES efforts in other parts of the global ocean (e.g., Anderson, 2019; Boyle et al., 2012), has not previously been accomplished in the China marginal seas.

In this study, we present dissolved trace metal (Fe, Ni, Cu, Zn, Cd, and Pb) concentration data in the China marginal seas, including YS and ECS, during the GEOTRACES GP06-CN cruise. Samples were collected from 8 vertical profiles, as well as at higher resolution in surface waters using an underway towfish. This greatly increases the spatial coverage of trace metal analyses in the China marginal seas, and for Zn represents the first reported data in this region. This new data highlights key aspects of the modern biogeochemical cycling of these elements, and by comparison to earlier datasets highlights the evolution of metal concentrations in China seas under anthropogenic influence over the past decades. The data thus may offer insight into metal cycling in coastal oceans and inform environmental management strategies.

2. Methods

2.1. Study region

The YS and ECS form part of the western Pacific marginal sea (Fig. 1). The YS is a semi-enclosed sea with a mean depth of 44 m, and the ECS is connected to the YS at the north with a broad continental shelf of approximately 640 km^2 and a mean depth of 72 m. The Yellow and East China Sea (YECS) area is heavily affected by Asian dust deposition,

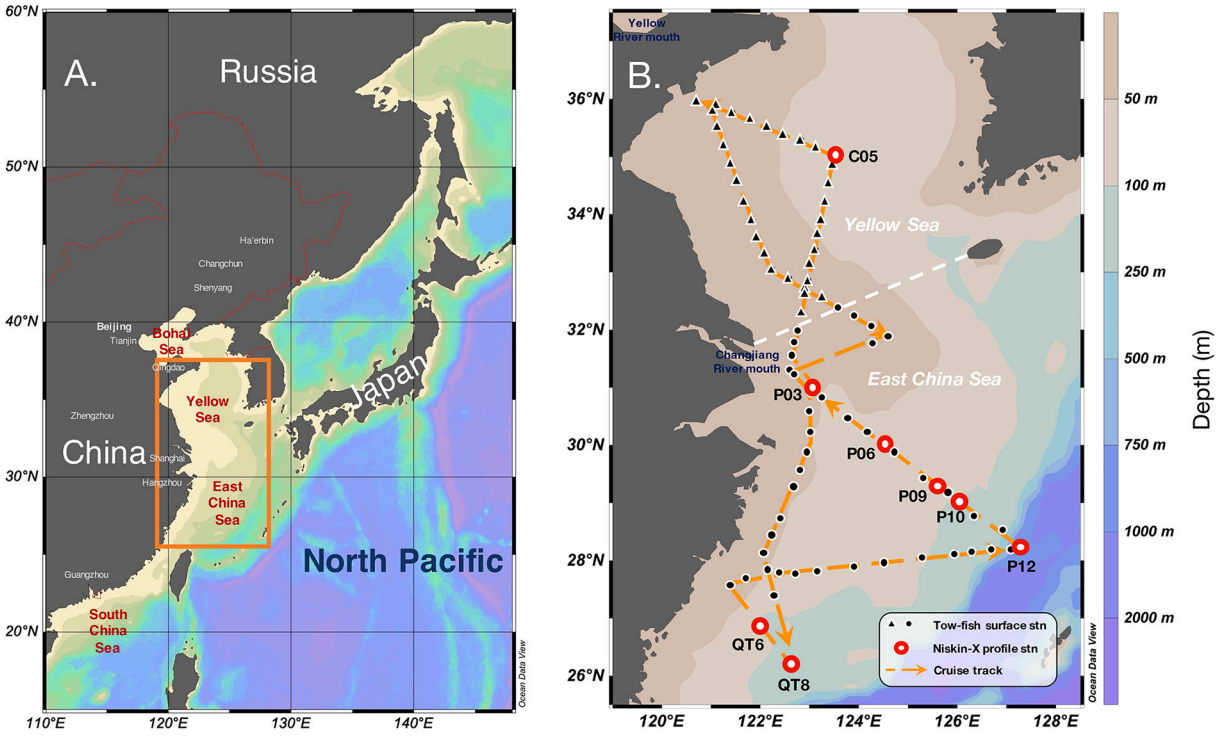

Fig. 1. Cruise information. A. Study area. Box shows our study area in the Yellow Sea (YS) and East China Sea (ECS). B. Station map. The white dashed line shows the rough historical definition on the boundary between YS and ECS which spans from the mouth of the Changjiang River to Cheju Island. The orange dashed line with arrowhead represents the cruise track. The black dots and triangles represent the towfish surface sampling locations: triangles represent the locations in the YS and circles represent those in the ECS. Red large circles represent the Niskin-X profile stations. (For interpretation of the references to colour in this figure legend, the reader is referred to the web version of this article.)

which is generated from inland deserts and may also mix with considerable anthropogenic emissions. The flux of Asian dust may have ecological impacts on the YECS (Fu et al., 2018; Guo et al., 2014). One of the major river freshwater sources to the YECS is the Changjiang (also called the Yangtze River) that accounts for approximately 90% of the total discharge of rivers into the YECS (Beardsley et al., 1985), and substantially inputs freshwater and chemical constituents into adjacent seas (Zhang, 1995). The YECS receives approximately 3 Gt of sediments per year, mainly from the Changjiang River, and from the Yellow River and the erosion of the old Yellow River mouth (Dong et al., 2011). The general circulation pattern in the YECS is shown in Fig. 2B, and has been described in previous studies (Su et al., 1994; Wu and Wu, 2018). The Changjiang River flows into the ECS, forming the highly dynamic Changjiang Diluted Water (CDW) system (Wu and Wu, 2018). The Kuroshio current (KC) is a strong boundary current in the northwest Pacific, and the main current flowing into and out of the YS and ECS has a surface speed of approximately 1 m s^{-1} (Su et al., 1994). The Taiwan Warm Current (TWC) is a dominant current that flows into the ECS to the north between 50 m and 100 m (Su et al., 1994). Along the coast, the Lubei Coastal Current (LBCC) carries water from the Bohai Sea into the YS southward. The Yellow Sea Coastal Current (YSCC) and the East China Sea Coastal Current (ECSCC) flow along the YS coast and the ECS coast southward, respectively.

The expedition for GEOTRACES GP06-CN was conducted on board the R/V Dongfanghong 2 in October 2015. As displayed in the cruise track shown in Fig. 1, the cruise sailed from Qingdao (36.1° N, 120.4° E) along the YS coast and the ECS coast toward the south, until it reached the southmost station QT8 in ECS, then turned back toward the near coast, across the ECS shelf to the east and reached the main stream of Kuroshio (Stn. P12). The cruise then sailed from Stn. P12 to Stn. P03 toward the Changjiang estuary (Fig. 1A), reached the YS station (Stn. C05), and finally sailed back to Qingdao.

2.2. Sample collection

Underway surface seawater was collected using a towfish system following the design reported by Vink et al. (2000) and Bruland et al. (2005), and deployed as described by Zhang et al. (2018). To avoid metal contamination, seawater collection was driven by an air-pressured teflon diaphragm pump, and the towfish was kept a certain distance away (5–7 m) from the side of the moving ship using a 6 m long boom. Acid cleaned Teflon-lined low density polyethylene tubing (TLP, Nalgene) was used to collect water samples at ~1 m of depth with the vessel moving speed of 8–10 knots. Seawater was directly pumped into a class-100 portable clean-flow bench at a flow-rate of ~6 L per minute, filtered through a 0.8/0.2 μm pore size AcroPak cartridge filter (Pall Corporation) in the wet lab on the vessel. The cartridge filter was flushed at least 2 min in prior to sample collection, and was swapped every 10 days depending on filtered volume. As described by Zhang et al. (2021), seawater depth profiles were collected at 8 stations using a non-metallic Kevlar line to suspend 12 L teflon-coated Niskin-X bottles (General Oceanics, FL USA) tripped with teflon-coated messengers. Once recovered on deck, Niskin-X bottles were relocated to a HEPA-filtered clean environment for sample filtering and collection. Seawater samples were immediately filtered through 0.8/0.2 μm Acropak filters (Pall Corporation) into a pre-acid-cleaned 250 mL LDPE bottle (Nalgene). The 250 mL filtered seawater samples were acidified to a pH of ~2 after the cruise using triple-distilled hydrochloric acid (HCl) in a clean lab at East China Normal University, and then stored for about two years before processing and analysis for dissolved trace metal concentrations. A certain storage time is required, especially for those trace metals (e.g. Cu) with organic binding complexes that may persist under acidic conditions for a certain time (Posacka et al., 2017). All plastic labware were precleaned followed the procedure described by Zhang et al. (2015a), first with a 2% citranox soak for 24 h, followed by hot leaching with 2 M HCl for 48 h, and then rinsing several times with 18.2 MΩ Milli-Q water and stored with 0.01 M triple-distilled HCl.

2.3. Dissolved metal concentration analysis

Seawater samples for dissolved trace metal (Fe, Ni, Cu, Zn, Cd, and Pb) concentration analysis were processed using a seaFAST pico (Elemental Scientific Inc.) in a clean room at University of Southern California (USC). Each 15 mL seawater subsample was amended with a mixture of metal isotope spikes (^{57}Fe, ^{62}Ni, ^{65}Cu, ^{67}Zn, ^{114}Cd, and ^{208}Pb), then processed according to a preprogrammed routine (Lagerström et al., 2013; Sohrin et al., 2008). Briefly, the seaFAST routine includes buffering samples to a higher pH (5–6), extraction of metals onto a Nobias resin column, rinsing with buffer to remove salts, and elution of metals with 5% HNO_3. 4 M ammonium acetate was used as the

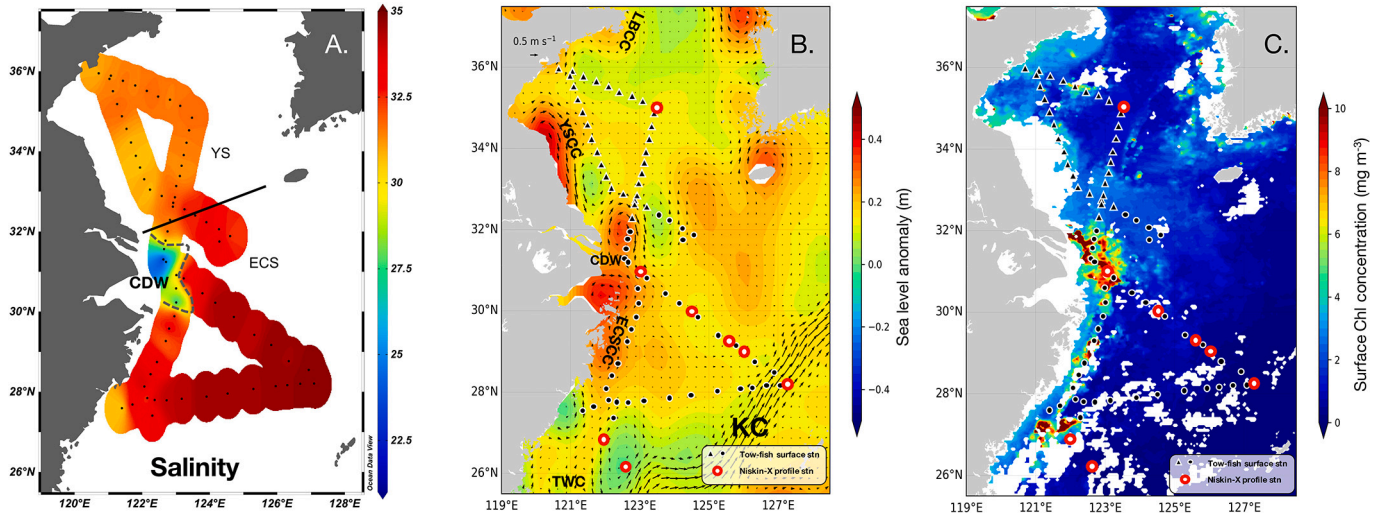

Fig. 2. Surface salinity (A) and satellite derived information during the cruise period (October 15 to 31, 2015). B. Sea level anomaly (colour) and flow pattern (arrows). C. Surface chlorophyll distribution. The black solid line shows the rough historical definition on the boundary between YS and ECS which spans from the mouth of the Changjiang River to Cheju Island. The black dots and triangles represent the towfish surface sampling locations: triangles represent the locations in the YS and circles represent those in the ECS. Red large circles represent the Niskin-X profile stations. Abbreviations: CDW = Changjiang Diluted Water; ECS = East China Sea; ECSCC = East China Sea Coastal Current; KC = Kuroshio current; LBCC = Lubei Coastal Current; TWC = Taiwan Warm Current; YS = Yellow Sea; YSCC = Yellow Sea Coastal Current. (For interpretation of the references to colour in this figure legend, the reader is referred to the web version of this article.)

buffer solution, which was made of a mixture of ultrapure water, ammonium hydroxide and acetic acid (optima grade, Fisher) and adjusting pH to 6.0 ± 0.2. Nitric acid used in this study was either purchased optima grade from Fisher, or double-distilled by a sub-distillation device (Savillex) with trace metal concentrations <10 ng g^{-1}. Samples were then analyzed on Element2 ICPMS at USC by isotope dilution as $^{56}Fe/^{57}Fe$, $^{60}Ni/^{62}Ni$, $^{63}Cu/^{65}Cu$, and $^{66}Zn/^{67}Zn$ in medium resolution, and $^{110}Cd/^{114}Cd$ and $^{207}Pb/^{208}Pb$ in low resolution, respectively. For Cd analysis, Pd and Sn isobaric interferences and polyatomic MoO+ interference were corrected following the procedure reported by John et al. (2018). The accuracy of the method was evaluated by running the GEOTRACES reference standard seawater, and the values were reported previously in Hawco et al. (2020). For this study, prior analyses of the GEOTRACES community reference standard SAFe D2 (D2–257) yielded concentrations of 1.06 nmol kg^{-1} Fe, 8.53 nmol kg^{-1} Ni, 2.36 nmol kg^{-1} Cu, 7.15 nmol kg^{-1} Zn, 1110 pmol kg^{-1} Cd, and 29.6 pmol kg^{-1} Pb. Milli-Q water adjusted to pH 2 was added every 15 samples to monitor the recovery efficiency and procedure blanks. The procedure blanks were 0.19 nmol kg^{-1}, 0.02 nmol kg^{-1}, 0.02 nmol kg^{-1}, 0.12 nmol kg^{-1}, 1.7 pmol kg^{-1} and 1.3 pmol kg^{-1} for Fe, Ni, Cu, Zn, Cd and Pb, respectively.

2.4. Supporting parameters

Physical and chemical parameters including salinity, temperature, dissolved oxygen, and phosphorous were acquired from the hydrographic and geochemical team of the GP06-CN cruise. Salinity and temperature were obtained using sensors on a CTD-rosette. Dissolved oxygen (DO) was measured via the Winkler titration method on board. Phosphorous was determined photometrically using an auto-analyzer (Model: Skalar SAN plus).

2.5. Satellite data

The satellite-derived data were averaged over our cruise period for intercomparisons between the biogeochemical and physical parameters. Satellite-based chlorophyll concentration data are obtained from the Moderate Resolution Imaging Spectroradiometer (MODIS) dataset (https://modis.gsfc.nasa.gov/). We used the Level-3 standard mapped chlorophyll concentration derived from measurements by satellite Terra, with a horizontal resolution of 4 km. To provide the background flow information during the cruise period, we used the sea-level anomaly and geostrophic current data from the Archiving, Validation and Interpretation of Satellite Oceanographic (AVISO) dataset (https://www.aviso.altimetry.fr), which has a horizontal resolution of 0.25°.

3. Results

3.1. Satellite-based circulation patterns and surface chlorophyll concentration

The satellite-based average flow pattern and surface chlorophyll concentrations during October 15 to 31, 2015 are shown in Fig. 2B. The satellite-based average flow pattern during the cruise period was consistent with the general flow patterns in the YECS, however no obvious TWC flow was observed on the surface. The satellite flow pattern suggested that freshwater from the Changjiang River flowed into the ECS and branched toward the south and the northeast. As shown in Fig. 2C, the averaged satellite-based surface chlorophyll showed a general distribution pattern of relatively higher concentrations in YS than ECS. Most chlorophyll values from our study area were lower than 2.0 mg m^{-3} off the coast, while high chlorophyll concentrations were observed along the coast and the shallow waters off the Changjiang estuary.

3.2. Surface distributions

Surface distributions of salinity and Fe, Ni, Cu, Zn, Cd, and Pb concentrations in the YS and ECS are shown in Table 1, Fig. 2A and Fig. 3. Of all 69 surface samples, the ECS had the most saline water, with an average salinity of 33.57 ± 1.09. Changjiang diluted water yielded the lowest level of salinity, averaging 26.92 ± 1.09, which was directly influenced by the Changjiang freshwater discharge. Averaged salinity in the YS was 31.49 ± 0.47, intermediate between the two other water masses. CDW yields salinity that is <30 in this study. All trace metals except Pb exhibited the lowest values in the ECS, with an average value of 3.15 ± 4.53 nmol kg^{-1}, 3.47 ± 0.73 nmol kg^{-1}, 3.99 ± 2.39 nmol kg^{-1}, 0.58 ± 0.34 nmol kg^{-1}, and 84 ± 57 pmol kg^{-1}, for Fe, Ni, Cu, Zn, and Cd, respectively. As shown in Fig. 3, the highest metals concentrations were recorded along the YS coast with the highest averaged concentrations in the YS, for example, Ni, Zn, and Cd recorded the highest concentrations in the YS in this study, averaging 6.96 ± 2.04 nmol kg^{-1}, 1.11 ± 0.39 nmol kg^{-1}, and 357 ± 119 pmol kg^{-1}, respectively. Fe and Cu recorded the highest concentration in the CDW, with an average value of 8.97 ± 3.54 nmol kg^{-1} and 12.68 ± 5.17 nmol kg^{-1}, respectively, which suggests a riverine source from the Changjiang River. The distribution pattern of Pb was notably different compared to other metals, with the highest values recorded in the ECS and lowest values in the YS. The average Pb concentration in the YS, CDW, and ECS were 61 ± 28 pmol kg^{-1}, 39 ± 15 pmol kg^{-1} and 72 ± 21 pmol kg^{-1}, respectively. At the furthest southwest towfish station (27.6° N, 121.4° E), elevated metal concentrations compared to the surrounding stations were observed, with the lower salinity at this location suggesting input from an end-member source with high metal concentrations and low salinity (Fig. 2A and Fig. 3).

3.3. Vertical distributions

The vertical distributions of salinity, temperature, apparent oxygen utilization (AOU), and dissolved trace metals during the GP06-CN cruise are shown in Fig. 4. On the continental shelf (< 200 m) of China marginal seas, the vertical distribution of salinity and temperature generally decreased from offshore to the Changjiang estuary. Water at a depth of 65 m at station C05 in the YS was cold (temperature = 9.92 °C) and salty (salinity = 33.13) (Su et al., 1994). Trace metals, except Pb, showed a generally increasing trend from offshore to nearshore. Similar to surface water, the highest trace metal concentrations were usually found in the YS. Station P12 was located in the main stream of Kuroshio current (Fig. 1B). Off of the continental shelf, Ni, Cu, and Cd exhibited a nutrient-like distribution pattern similar to the pattern of AOU, with low concentrations at the surface and increasing concentrations with increasing depth. Fe and Zn showed a hybrid distribution pattern at Station P12 (Bruland and Lohan, 2006), with a surface water maxima, then a minimum in the subsurface and finally increasing values at greater depth similar to a nutrient-type distribution.

No clear vertical distribution pattern was observed for Pb among the 8 profiles in this study. However, surface maximum values were usually observed, with exceptions of stations QT6 and QT8, at which subsurface or bottom maxima were observed. Dissolved Pb vertical profile at station P12 showed a maximum value of 67 pmol kg^{-1} at the surface, a subsurface minima of ~44 pmol kg^{1} at depths ranging from 85 m to 100 m, an increase to 68 pmol kg^{-1} at 400 m, and then a decrease at greater depths, with a minimum value of 34 pmol kg^{-1} at the depth of 800 m.

4. Discussion

4.1. Distinct trace metal distribution patterns

By studying many trace metals together, we can gain a more comprehensive understanding of the processes which impact each element across the marginal seas, with some processes affecting several

Table 1
Dissolved trace metals in surface waters of the Yellow Sea and the East China Sea (Fe, Ni, Cu, and Zn in nmol kg^{-1}, Cd and Pb in pmol kg^{-1}).

	Yellow Sea				Changjiang diluted water				East China Sea			
	min	max	*Average*	*1σ, n = 28*	*min*	*max*	*average*	*1σ, n = 6*	*min*	*max*	*Average*	*1σ, n = 35*
Salinity	30.60	32.80	31.49	0.47	22.00	29.70	26.92	2.75	30.60	34.80	33.57	1.09
Fe	0.82	37.92	5.88	7.57	4.31	14.39	8.97	3.54	0.41	24.83	3.15	4.53
Ni	4.37	10.32	6.96	2.04	4.79	6.10	5.51	0.54	2.25	5.08	3.47	0.73
Cu	7.04	19.13	10.6	3.57	6.19	20.58	12.68	5.17	0.53	11.25	3.99	2.39
Zn	0.41	1.92	1.11	0.39	0.20	1.02	0.70	0.27	0.15	1.62	0.58	0.34
Cd	177	614	357	119	138	267	205	51	2	227	84	57
Pb	32	126	61	28	24	67	39	15	43	126	72	21

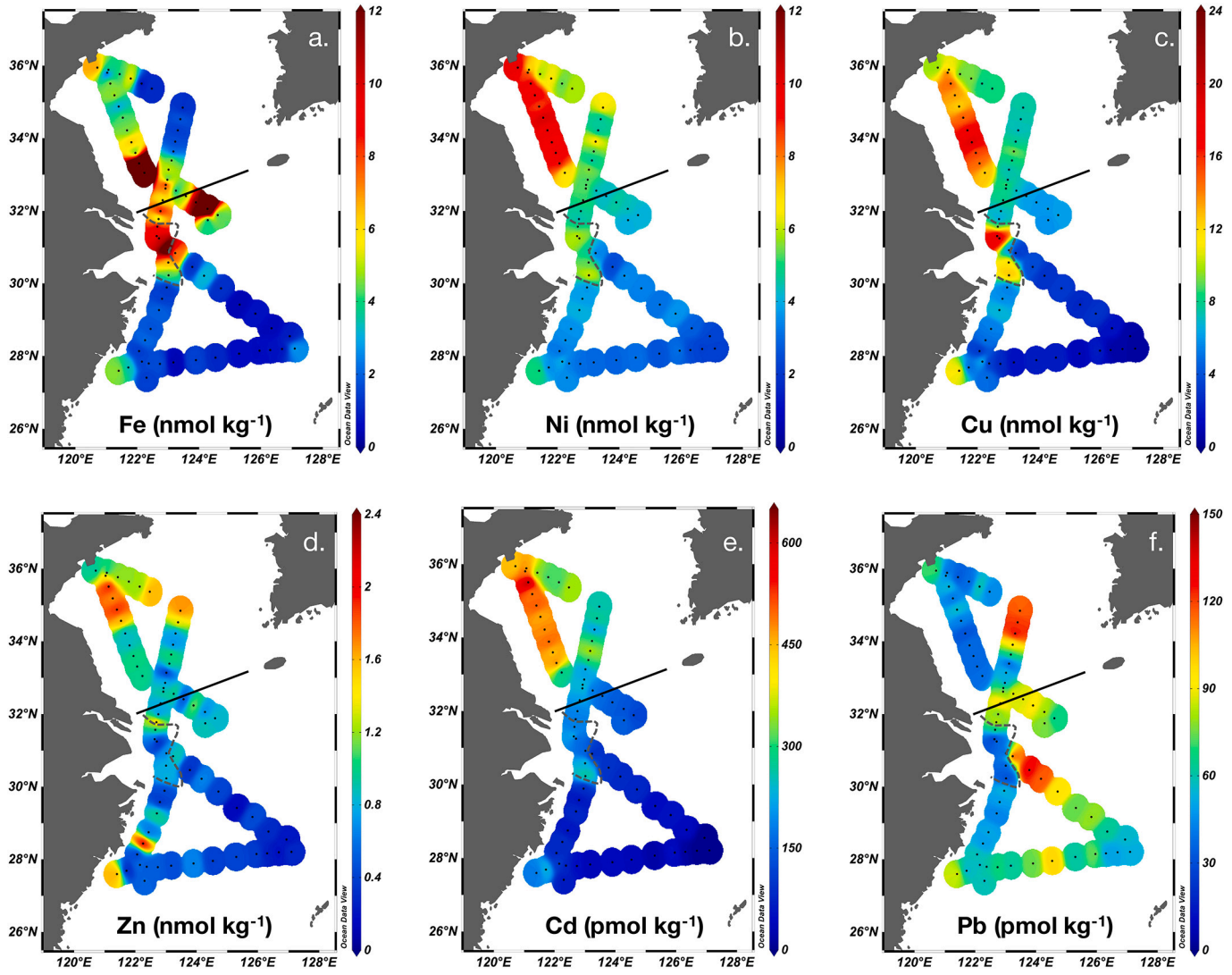

Fig. 3. Surface distribution of trace metal (Fe, Ni, Cu, Zn, Cd, and Pb) concentrations in the Yellow Sea and East China Sea during the GP06-CN cruise. (For interpretation of the references to colour in this figure legend, the reader is referred to the web version of this article.)

elements similarly, and other processes affecting just one metal. Comparing metal concentrations to salinity provides a first-order understanding of which elements are most heavily impacted by fluvial input (Fig. 5). The generally negative correlation between Fe, Ni, Cu, Zn, and Cd, and salinity in surface waters suggests that riverine input and mixing among different endmembers were dominant processes in the YECS. Conversely, Pb was not correlated with salinity, highlighting its unique behavior among all investigated trace metals. In addition to a strong salinity signal, Fe and Zn appear to undergo more complex biogeochemical cycling processes, giving them a distinct distribution patterns compared to that of Ni, Cu and Cd (Fig. 3 and Fig. 5). Key processes impacting each of these trace metals in the YECS will be discussed in the following subsections.

4.1.1. Ni, Cu, and Cd are dominated by mixing and regeneration

Ni, Cu and Cd each had a nearly linear slope when plotted against salinity at surface in the ECS and CDW, respectively, suggesting the dominant control of mixing between the freshwater high-metal Changjiang River endmember and a more saline low-metal water endmember from the northwestern Pacific that is carried by the Kuroshio, one of the

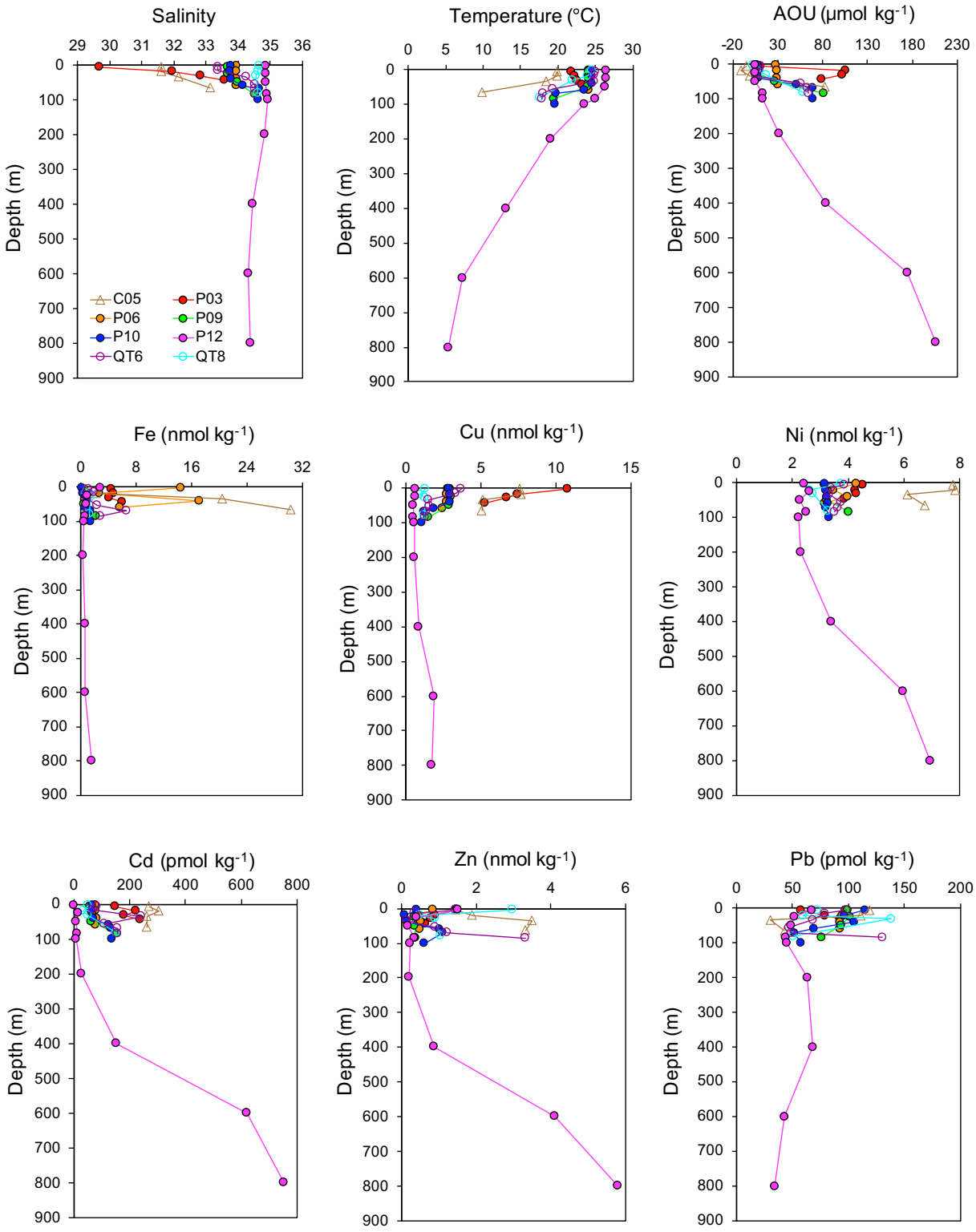

Fig. 4. Salinity, temperature (°C), apparent oxygen utilization (AOU, μmol L^{-1}), and dissolved trace metal concentrations in the water column of the YS and ECS (Fe, Ni, Cu, and Zn in nmol kg^{-1}, Cd and Pb in pmol kg^{-1}).

largest western boundary currents in the world. The intercepts suggested for Changjiang freshwater endmember (salinity of 0) were 14 nmol kg^{-1}, and 53 nmol kg^{-1} for Ni and Cu, respectively. These values are consistent with the range reported at the Xuliujing station (Yin et al., 2015), the nearest upper reaches before Changjiang freshwater meets ECS seawater. For Cd, the calculated intercept at 735 pmol $kg^{-1}$for Cd is well above the earlier reported range of its river endmember (Yin et al., 2015). However, this can be attributed to the fact that Cd is well known to desorb from particles during river and seawater mixing in the estuary (Boyle et al., 1982; Comans and van Dijk, 1988). The conservative behavior of Cd in surface waters along CDW to ECS is consistent with that observed by Edmond et al. (1985), who indicated that Cd

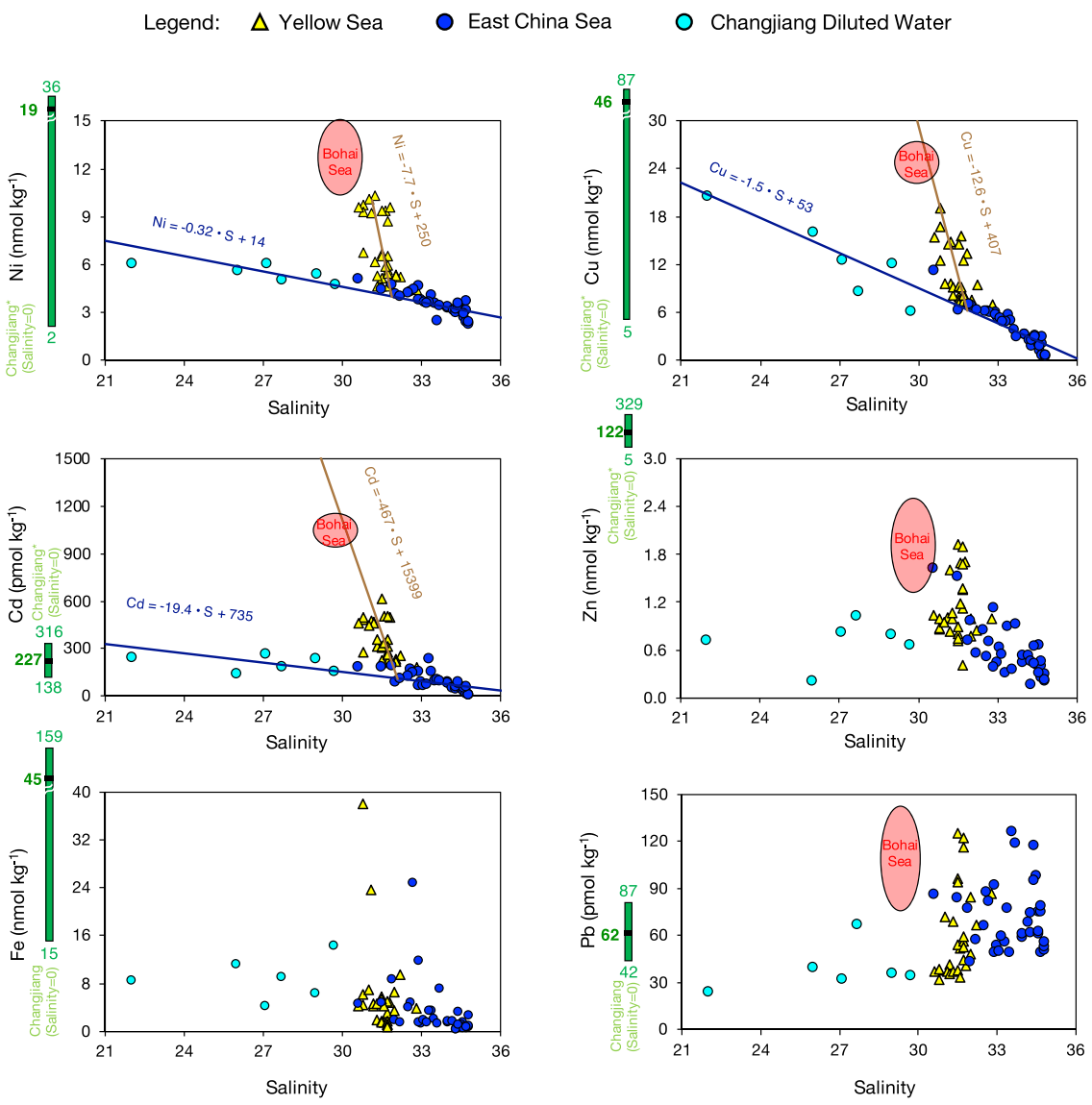

Fig. 5. Trace metals (Fe, Ni, Cu, Zn, Cd, and Pb) versus salinity in the Changjiang diluted water (light blue circles), the ECS (dark blue circles), and YS (yellow triangles) from towfish surface sampling during the GP06-CN cruise. Green bars and numbers beside the y-axis of each metals show the range of trace metal concentrations from the Changjiang freshwater endmembers, black lines and numbers in bar represent the average values. The endmember concentrations at Xuliujing are extracted from Ni, Cu, Cd, and Zn (Yin et al., 2015), Fe (Zhu et al., 2018), Pb (Jiang et al., 2018), ellipses shows the range of metals and salinity in the Bohai Sea reported by Li et al. (2015). (For interpretation of the references to colour in this figure legend, the reader is referred to the web version of this article.)

experienced a desorption step at low salinity, followed by conservative behavior as salinity increased further. In the YS surface waters, Ni, Cu, and Cd can also be considered as a mixing of two endmembers between the moderate-salinity/moderate-metal concentrations (salinity ranged from ~31 to 33) in the ECS and the low-salinity/high-metal waters originating from the Bohai Sea (Li et al., 2015). The high trace metal concentrations in the YS thus indicate either high concentration riverine endmembers (e.g. Yellow River) or heavy metal pollution around the Bohai Sea (Su et al., 1994; Wang et al., 2018).

In order to better understand the role of biological uptake and remineralization of metals, concentrations of Ni, Cu, Cd, and phosphate (P) were plotted against both salinity and AOU, for water column samples collected at depth profiles (Fig. 6). As illustrated by P, a coupling with AOU but decoupling with salinity is indicative of a nutrient controlled by uptake in surface waters and remineralization from settling particles at depth. Thus, in addition to mixing pattern at surface ECS, the similar distribution pattern of Cd compared to P is not surprising, owing to its nutrient-type distribution observed in early years (Boyle et al., 1976), and the application of pairing Cd—P as tracer in various marine environments (Boyle, 1988; de Baar et al., 1994; Middag et al., 2018; Zhang et al., 2019). Surprisingly, the relationship between Cu and salinity was similar throughout the ECS shelf both in surface water towfish samples and full water column depth profiles. Given a residence time of ~1 year for shelf water in the ECS (Chen, 1996), the residence time of riverine Cu must be longer than that of the water on the ECS shelf to exhibit conservative behavior on the shelf. Only one species of strong Cu binding ligand was observed in the southern YS (Li et al., 2017), but this organic complexation may help Cu to persist for a long residence time in YECS. The pattern for Ni lies between that of Cd and Cu, suggesting that both mixing and regeneration significantly impact Ni distributions in the water column. The apparent coupling of these metals with salinity and/or biological cycling is caused primarily by the magnitude of difference between their endmembers. For example, the Cu concentration difference between ~50 nmol kg^{-1} in Changjiang and ~ 1 nmol kg^{-1} from the northwest Pacific is two orders of magnitude, while for Ni the concentration difference is just 4-fold between

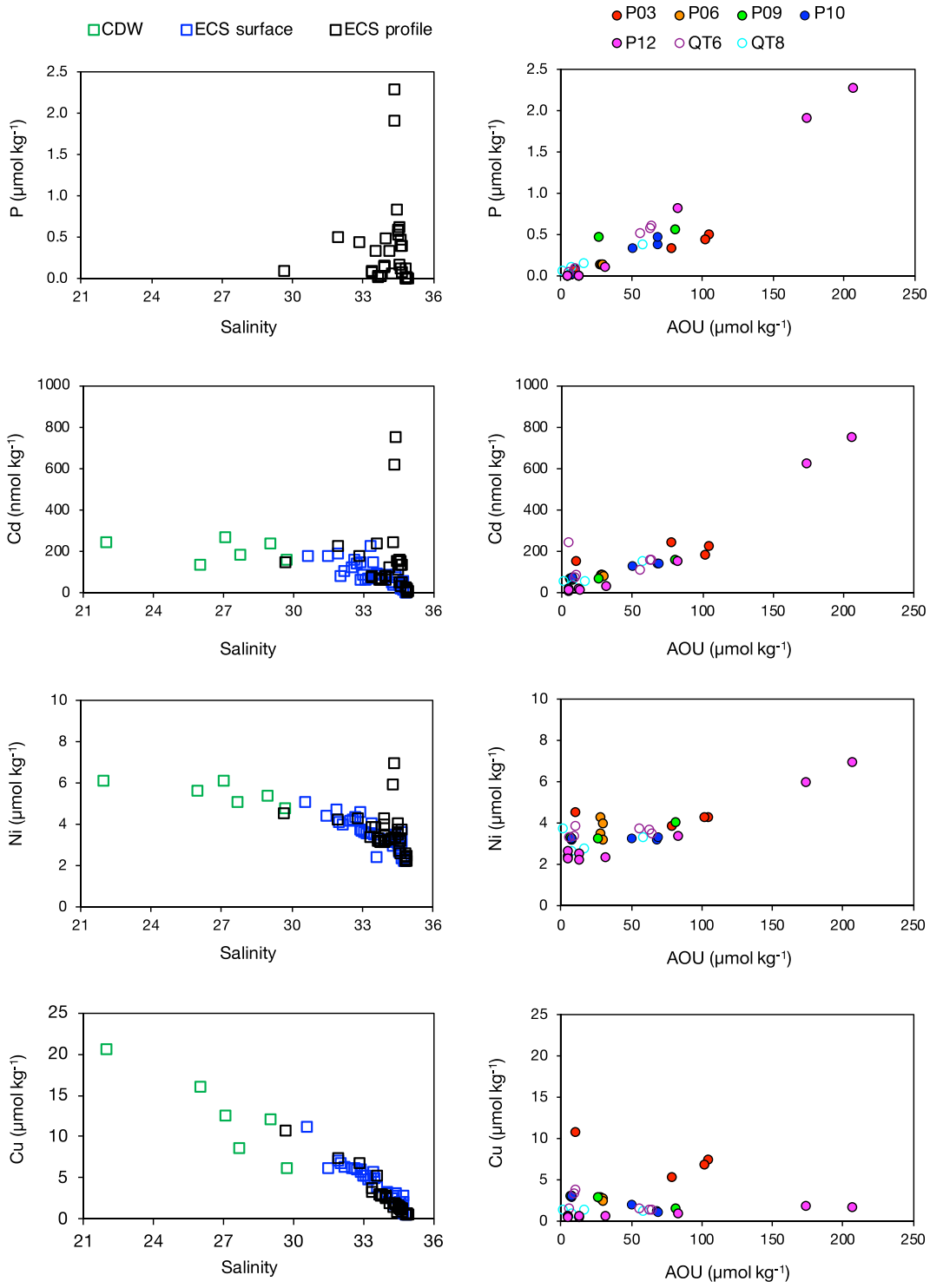

Fig. 6. Phosphate (P), Cd, Ni, and Cu versus salinity in both surface water in Changjiang Diluted Water (CDW) and the ECS, and profile samples in the ECS. P, Cd, Ni and Cu versus AOU at profile stations in the ECS.

~20 nmol kg^{-1} in the riverine endmember and ~ 5 nmol kg^{-1} in seawater from the northwest Pacific, and concentrations are indistinguishable (~several hundreds pmol kg^{-1}) between the two endmembers for Cd.

As a robust relationship was observed between Cu and salinity throughout the ECS water body, we discuss the potential role of Cu as a tracer of both natural geochemical processes and anthropogenic processes. Previous studies have also reported the strong correlation between Cu and salinity in the YECS (Abe et al., 2003), the Japan Sea (Kang et al., 2014), and the western subtropical Atlantic (Roshan and Wu, 2015). Among these three studies, the inferred freshwater Cu concentration based upon the intercept of Cu versus salinity was highest in the ECS at 74 nmol kg^{-1}, was 55 nmol kg^{-1} in the Japan Sea, and 39 nmol kg^{-1} in the western subtropical Atlantic. Our inferred freshwater intercept of 53 nmol kg^{-1} Cu for the ECS, along with the recent Cu concentration reported in Changjiang (Yin et al., 2015), both exceeded

the range of 18–21 nmol kg^{-1} measured in the Changjiang in 1985 (Edmond et al., 1985). Cu concentrations in the Changjiang are presumably influenced by rock type and weathering regimes, however lower Cu concentrations observed in the Changjiang decades ago (Edmond et al., 1985) suggests that anthropogenic activity is likely responsible for much of the high Cu content observed in this study.

In summary, the abundance of Ni, Cu, and Cd is mostly attributed to mixing and biological uptake/regeneration in the YECS. Our data support the conservative behavior of Ni and Cu in the estuary (Boyle et al., 1982; Edmond et al., 1985; Windom et al., 1988). Previous estimates have suggested that fluvial inputs of Ni and Cu contribute 94% and 89% of the ocean fluxes, respectively (Ciscato et al., 2018; Little et al., 2014). Our data support such conclusions that rivers are the main source of Ni and Cu in the ocean. The dominant role of riverine discharge in the coastal ocean is evident, despite the nearby presence of other potential sources such as sedimentary flux and atmospheric deposition.

4.1.2. *Recent atmospheric input fingerprint for surface Pb*

Unlike other metals, Pb in the YECS did not show any correlation with salinity (Fig. 5). Pb concentrations measured in this study are consistent with other recent data for the YECS (24–96 pmol kg^{-1}, Jiang et al., 2018) and the India marginal seas (42–82 pmol kg^{-1}, Echegoyen et al., 2014). Zhang (1995) suggested conservative behavior of Pb in the Changjiang estuary, however a comparison of our CDW data (averaging 39 pmol kg^{-1}) with recent data on river water endmembers (averaging 62 pmol kg^{-1}, Jiang et al., 2018) suggests a removal of Pb from the Changjiang across the estuary. The Pb concentrations in the YECS cannot be easily accounted for by mixing with any nearby endmembers, including the Changjiang (Jiang et al., 2018) and Bohai Sea (Li et al., 2015). Instead, Pb concentrations in the Yellow Sea Coastal Current that are close to terrestrial sources was low, while Pb concentrations further offshore in the ECS offshore were higher.

The distinctive distribution pattern of Pb in the YECS is therefore attributed to recent atmospheric deposition, and the short residence time of Pb in surface waters. This is based on two features we observed during the GP06-CN cruise. First, in the deep water column Pb profile at Station P12 on the mainstream of Kuroshio, a surface maximum of 67 pmol kg^{-1} Pb was observed (Fig. 4), which is notably different from the low surface ocean Pb values seen in Pb profiles at the Hawaii-HOT station in the subtropical Pacific gyre (35 pmol kg^{-1}, Boyle et al., 2005), and at the same location in a recent study (41 pmol kg^{-1}, Jiang et al., 2018). We do not believe that the high surface ocean Pb concentrations measured here are due to contamination, because our five data points exhibit a smooth and oceanographically consistent distribution pattern in the upper 100 m. This pattern could be interpreted either as mixing between high values at the surface and low values at 50–100 m, or scavenging of Pb from the subsurface. Data points at depths below 50 m are consistent with values reported in the North Pacific in previous studies (Boyle et al., 2005; Jiang et al., 2018). Secondly, the 10 m 48 h aerosols back trajectory (Stein et al., 2015) from several stations along the cruise track clearly showed that high surface Pb values in the YECS were associated with back trajectories which crossed industrial areas of the Chinese mainland (Fig. 7). Aerosol lead emission are concentrated in eastern and central China due to the high level of coal consumption, non-ferrous metal smelting and from other industries such as lead-acid battery manufacturing (Li et al., 2012; Liu et al., 2017). Conversely, lower Pb concentrations were associated with back trajectories over the open oceans. Pb distribution pattern is also comparable to the averaged aerosol optical thickness (AOT) distribution over our sampling period, particularly at the offshore stations (Fig. S1, see in the supplementary information). Therefore, we conclude that Pb surface maxima most likely result from recent input of Pb by atmospheric deposition.

The impact of recent atmospheric deposition on surface ocean Pb concentrations suggests a very short residence time of Pb in surface waters. The residence time of Pb in the surface waters of oligotrophic ocean gyres ranges from months to years (Boyle et al., 2005; Bridgestock et al., 2016). If the Pb residence time in the YECS were similarly long, considering a residence time of ~1 year of shelf water in the ECS (Chen, 1996), we would expect Pb concentrations to reflect mixing among different water masses rather than the high spatial variation we observed. However, recent observations suggest a shorter residence time of Pb in surface waters, especially in nearshore locations (Bridgestock et al., 2016; Echegoyen et al., 2014). Pb isotope data in sediment cores shows that aerosol deposition of anthropogenic Pb from coal burning is the dominant source of Pb to the East China Sea shelf (Wang et al., 2014). Given the short residence time of anthropogenic aerosols (~days, (Rastogi and Sarin, 2013)), high Pb enrichment in Chinese aerosols (Zhang et al., 2017; Zhao et al., 2015a, 2015b), and fast Pb dissolution of anthropogenic aerosols in seawater (Mackey et al., 2015, ~46% of bulk Pb after 10 min), our data therefore suggest that the residence time of Pb in the China marginal seas is much shorter than in oligotrophic gyres (days to weeks, rather than weeks to years). This may be due both to differences in the source of Pb to these waters, and to differences in scavenging loss of Pb in productive coastal waters.

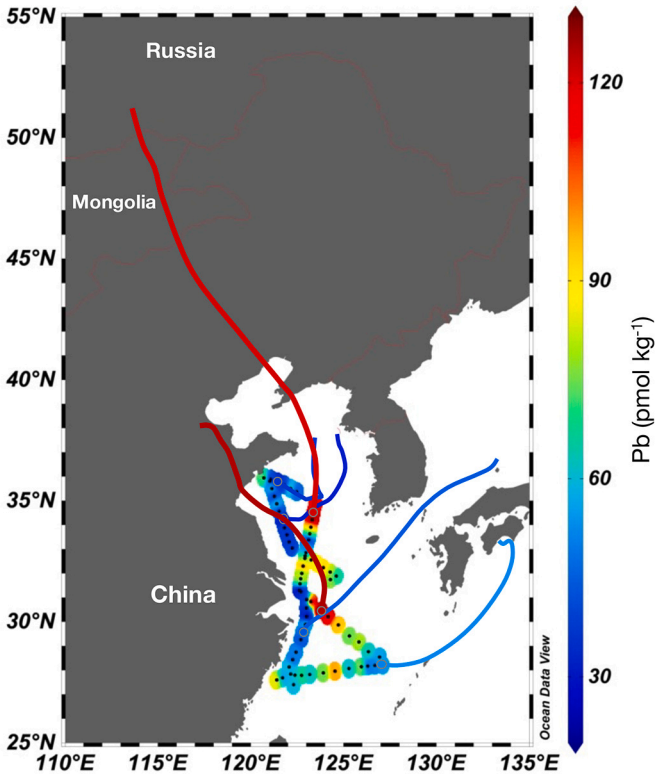

Fig. 7. 10 m aerosol back trajectory for 48 h preceding the sampling along the cruise track on the surface dissolved Pb distributions in the YS and ECS. Colors in each track line correspond to the surface dissolved Pb concentration according to the colour bar beside the maps.

4.1.3. *Complex cycling of Fe and Zn*

Fe is likely the most studied trace metal in the marine environment, owing to the significant role it plays in regulating marine primary production, and the complexity of its biogeochemical cycling. Efforts to constrain the flux of Fe from various Fe sources to the ocean, and to quantify the internal cycling of Fe within the oceans, face challenges; for example, see discussions on what controls dissolved iron in the world ocean (Boyle, 1997; Johnson et al., 1997; Sunda, 1997), and the synthesis reviews on marine Fe biogeochemistry (Boyd and Ellwood, 2010; Tagliabue et al., 2017). Zn cycling in the oceans is also complex, reflecting multiple possible sources to the ocean (Lemaitre et al., 2020; Little et al., 2014) and internal cycling processes which may include biological uptake and remineralization, and scavenging (John and

Conway, 2014; Vance et al., 2017; Weber et al., 2018).

While there is an overall negative correlation between Fe concentrations and salinity which suggests fluvial input, the weak coupling between these two demonstrates that other processes are also quite important in Fe biogeochemical cycling. Biological Fe uptake and regeneration seem to be one of these additional processes. We used the observed AOU:Fe relationship to calculate the regenerated Fe:C ratios, applying a molar AOU:C ratio of 1.6, typical for marine phytoplankton (Sunda, 1997). The Fe:C ratio derived from the correlation of Fe and AOU at Station P12 on the main stream of Kuroshio is similar to those observed in the North Pacific (Fig. 8) (Sunda, 1997). On the ECS shelf, however, the Fe:AOU ratios are much higher than at the offshore P12 station, suggesting the presence of other Fe sources on the shelf, or that the regeneration of biologically derived particles yields a relatively high Fe:C ratio. Indeed, luxury uptake by marine biotas is usually observed in high-Fe marine environments (Fitzsimmons et al., 2013; Sunda and Huntsman, 1995). We similarly compared Fe concentrations to those of dissolved phosphate to better understand the role of biological Fe cycling, and for comparison to Fe:P ratios measured for cultured marine phytoplankton (Ho et al., 2003). Some of our observed values exceeded the highest Fe:P ratio found in prasinophyceae species (Ho et al., 2003), as shown in Fig. 8. Besides riverine input, mixing, and regeneration of biological particles, we therefore infer other significant fluxes of Fe into the China marginal seas, which may include sedimentary flux (Liao and Ho, 2018), atmospheric deposition (Guo et al., 2014), and desorption of Fe from fluvial particles (Zhu et al., 2018). As estimated by a recent study (Zhang et al., 2022), Fe sources including Changjiang discharge, dry and wet atmospheric deposition, dissolution from sediments, and the western boundary current were all found to have significant and comparable contributions to Fe budgets on the ECS. Large uncertainties within the multiple Fe sources revealed by Zhang et al., 2022 also support the complexity of Fe biogeochemical cycling observed in this study. Both budgets estimation and process study are required for a further understanding of the Fe biogeochemical cycles in the ocean.

Similarly, the distribution of Zn suggests a complex mix of processes. For example, the concentration of Zn in the surface Yellow Sea is high in the most northeastern corner or the transect, at a location where Ni, Cu and Cd are not particularly elevated, but where a clear Pb maximum was observed (Fig. 3). This suggests a possible Zn source from atmospheric deposition into the YS, which is corroborative with the recent recognition of the importance of anthropogenic aerosol Zn to the ocean (Liao et al., 2021). However, this did not lead to a very large buildup in surface ocean Zn concentrations at the sites where high Pb content was observed, which could be attributed to a higher biological demand for Zn than Pb, different Zn and Pb contents in aerosols from various origins, or differences in the solubility of aerosol Zn and Pb (Mahowald et al., 2018; Morel and Price, 2003). Elevated near-surface Zn concentrations observed in both surface distributions and profiles suggest additional Zn sources to the region including sedimentary input and fluvial input (Figs. 2, 3). A recent evaluated aerosol Zn flux to the ocean was found that is comparable to the output magnitude from hydrothermal and riverine sources (Liao et al., 2021).

4.2. Historical observations of trace metals in the Yellow Sea and East China Sea

Comparison of our data with several historical datasets allow us to study the evolution of trace metals in China's marginal seas during the past three decades (Fig. 9), including previous studies of Cu, Ni, Cd and Pb in the YECS (Abe et al., 2003; Jiang et al., 2018; Jiann et al., 2009). Extensive industrialization and urbanization activities began in China in the late 1980's, with notable increases in environmental pollution emissions associated with rapid economic growth, though overall levels of pollution in China have generally declined since ~2000 (Hu et al., 2014). Only Cu data can be compared during a period of 20 years, and our data show an increase in Cu pollution in the YECS between 1995 and 2015. Though, due to limited historical data, other pollutant metals do not appear to have significantly increased in concentration with a short time span.

End-member concentration of metals in freshwater riverine input can be determined from a regression between metal concentrations and salinity. The regression slope of Ni against salinity in the ECS yield different values over the span of 11 years, at −0.68 in 2004 (Jiann et al., 2009) and − 0.58 in 2015 (this study), though the difference was not statistically significant (*t*-test, 95% confidence level). Inferred Ni riverine end-member concentrations were 26.31 ± 1.64 nmol kg^{-1} in 2004 and 22.84 ± 1.97 nmol kg^{-1} in 2015 (all errors 2σ SE). Similarly, the relationship between Cd and salinity yielded slopes which were not significantly different (t-test, 95% confidence level), at −39 in 2004 (Jiann et al., 2009) and −40 in 2015 (this study). Inferred Cd riverine end-member concentrations were 1396 ± 194 pmol kg^{-1} in 2004 and 1438 ± 196 pmol kg^{-1} in 2015.

Levels of anthropogenic Pb contamination in China have changed significantly over the recent decades. Pb contamination from automobiles decreased after policies on unleaded gasoline were started in late 1990s in China (Jiang et al., 2018), though Pb emission from other industries such as lead-acid battery manufacturing increased due to China's economic growth (Liu et al., 2017). An increased trend for Pb pollution after 2010 has been observed in sediment profiles from the ECS (Sun et al., 2019). Unfortunately, however, data are only available over a two year span for ECS seawater Pb concentrations, from studies sampled in 2013 and 2015 (Jiang et al., 2018; this study), and the regression with salinity showed no statistically significant difference between those years. Fe is usually considered as macro nutrients to

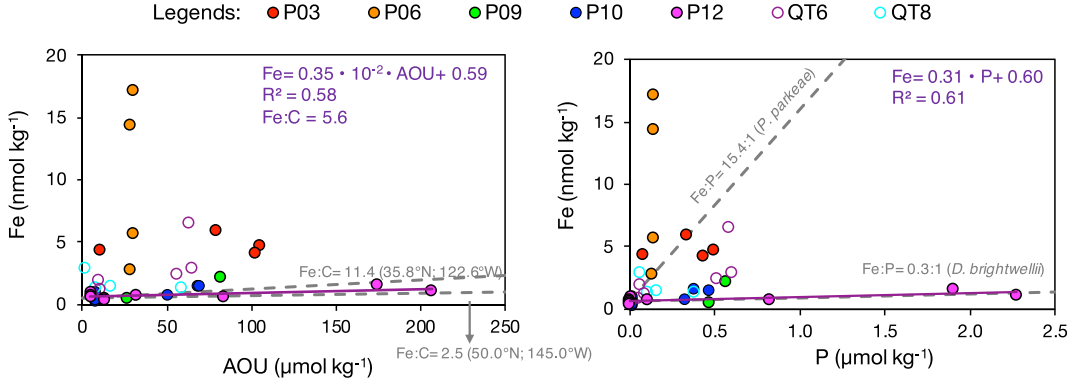

Fig. 8. Fe versus AOU (left panel), and phosphate (right panel) in the water column during the GP06-CN cruise. Fe to C ratios from two North Pacific stations (Sunda, 1997) are plotted using dashed lines in the left panel to compare with the Fe:C ratio derived from the Fe:AOU ratio at Station P12 from this study. Fe to P ratios obtained from the study of Ho et al. (2003) are plotted using dashed lines in the right panel to compare with the Fe:P ratio at Station P12 from this study.

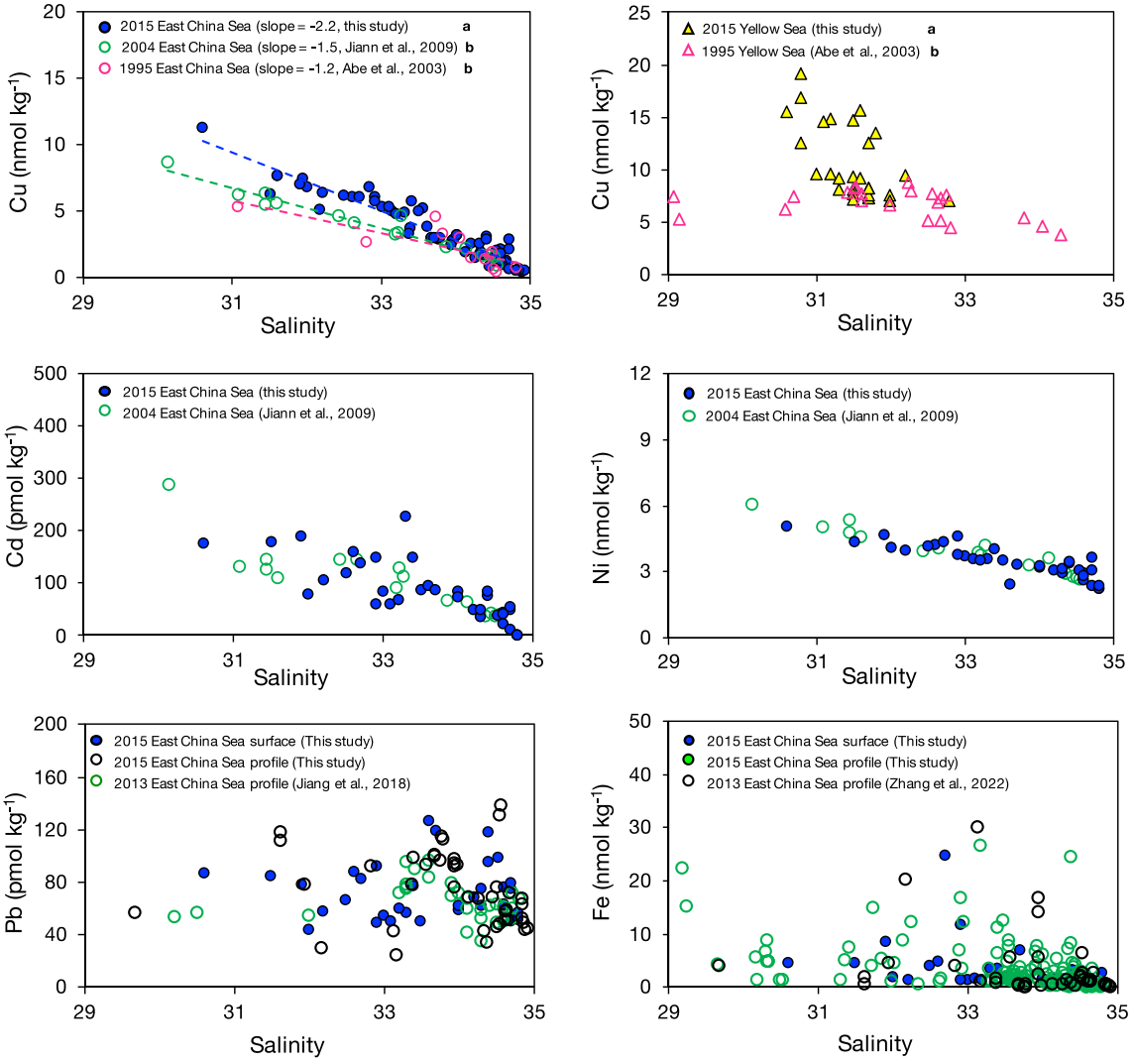

Fig. 9. Historical dissolved trace metal (Cu, Ni, Cd, Pb and Fe) concentrations versus salinity in the YS and ECS, including data from this study and previous studies (Abe et al., 2003; Jiang et al., 2018; Jiann et al., 2009; Zhang et al., 2022). Regression coefficients of Cu compared to salinity which are denoted by the same letters (a or b) for each data set are not significantly different at $p < 0.05$ (*t*-test).

marine biota. Recent study has been suggested that the anthropogenic Fe may fuel primary production in the ocean (Pinedo-Gonzalez et al., 2020). Comparable Fe concentrations were observed in ECS seawater from studies sampled in 2013 and 2015 (Zhang et al., 2022; this study).

There is a longer record of Cu sampling in the YECS, spanning 20 years, with samples collected in 1995, 2005, and 2015 (Abe et al., 2003; Jiann et al., 2009; this study). Inferred riverine end-member concentrations have increased over this time-period, from 42.74 ± 9.74 nmol kg^{-1} in 1995 to 53.90 ± 2.88 nmol kg^{-1} in 2004, to 74.20 ± 3.84 nmol kg^{-1} in 2015 (all errors 2σ SE) in the ECS and from 36.70 ± 8.69 nmol kg^{-1} in 1995 to 154.20 ± 37.39 nmol kg^{-1} in 2015 in the YS (Fig. 9). Urban development and the related industries such as cement production may be responsible for the anthropogenic Cu pollution (Zhang et al., 2015b). Indeed, Cu was found to be the most polluted metal in marine sediment in the China coast (Fang et al., 2009; Zhang et al., 2020). Observations from sediment profiles in the ECS suggested an increase in anthropogenic Cu from 1990s, followed by a gradual decrease of anthropogenic Cu starting in 2010 (Sun et al., 2019). Our observations confirm increased levels of Cu pollution over the past decades, and demonstrate the potential application of Cu as tracer for evolution of anthropogenic input in coastal oceans.

5. Conclusions

Marginal seas connect the land and open ocean, and receive both anthropogenic and natural inputs. Understanding trace metal cycling in the coastal oceans, where terrestrial and oceanic substance are exchanged, modified, and finally transported to the open ocean basin is important. The underway sampling of multiple trace-metals allows for the identification of metal behaviors in the highly dynamic China marginal seas, and the elucidation of their fate from land to the sea. Six metals were analyzed from samples collected during the GEOTRACES GP06-CN cruise, including Fe, Zn, Pb, Ni, Cu, and Cd. Of these we identified Ni, Cu, and Cd as coming mainly from fluvial inputs, with distributions reflecting both mixing between riverine and ocean end-members, and biological uptake and regeneration. We observed a patchy Pb distribution in Chinese coastal oceans, consistent with the recent atmospheric Pb input and its short residence time in surface waters. The distributions of Fe and Zn were impacted by multiple different sources and sinks, and internal cycling. Comparison with historical data suggested that Cu concentrations can trace a historical increase in anthropogenic Cu inputs to the YECS from rivers. Pb can be used to reveal the recent atmospheric deposition, however, the residence time of atmospheric input at different locations should be further constrained. For Fe

and Zn, a complete understanding of their distribution requires a better understanding on their modification in the marginal seas and the contribution from various sources.

Declaration of Competing Interest

The authors declare that they have no known competing financial interests or personal relationships that could have appeared to influence the work reported in this paper.

Acknowledgments

We thank the captain and crew of R/V Dongfanghong 2 for the success of this expedition. We thank Drs. Huijun He and Lei Li for seawater sample collection and filtration on board, Dr. Jinnan Wu for statistical analysis. This work was supported by the National Natural Science Foundation of China (Nos. 41921006, 41861134040, 42076227). John was funded by NSF award OCE-1736896. The authors gratefully acknowledge the NOAA Air Resources Laboratory (ARL) for the provision of the HYSPLIT transport and dispersion model and/or READY website (http://www.ready.noaa.gov) used in this publication.

Appendix A. Supplementary data

Supplementary data to this article can be found online at https://doi.org/10.1016/j.chemgeo.2022.120948.

References

Abe, K., Ishihi, Y., Watanabe, Y., 2003. Dissolved copper in the Yellow Sea and the East China Sea - Cu as a tracer of the Changjiang discharge. Deep. Res. Part II Top. Stud. Oceanogr. 50, 327–337. https://doi.org/10.1016/S0967-0645(02)00457-5.

Anderson, R.F., 2019. GEOTRACES: accelerating research on the marine biogeochemical cycles of trace elements and their isotopes. Annu. Rev. Mar. Sci. 12.

de Baar, H.J.W., Saager, P.M., Nolting, R.F., van der Meer, J., 1994. Cadmium versus phosphate in the world ocean. Mar. Chem. 46, 261–281. https://doi.org/10.1016/0304-4203(94)90082-5.

Beardsley, R.C., Limeburner, R., Yu, H., Cannon, G.A., 1985. Discharge of the Changjiang (Yangtze River) into the East China Sea. Cont. Shelf Res. 4, 57–76.

Boyd, P.W., Ellwood, M.J., 2010. The biogeochemical cycle of iron in the ocean. Nat. Geosci. 3, 675–682. https://doi.org/10.1038/ngeo964.

Boyd, P.W., Jickells, T., Law, C.S., Blain, S., Boyle, E.A., Buesseler, K.O., Coale, K.H., Cullen, J.J., De Baar, H.J.W., Follows, M., Harvey, M., Lancelot, C., Levasseur, M., Owens, N.P.J., Pollard, R., Rivkin, R.B., Sarmiento, J., Schoemann, V., Smetacek, V., Takeda, S., Tsuda, A., Turner, S., Watson, A.J., 2007. Mesoscale iron enrichment experiments 1993–2005: synthesis and future directions. Science 80. https://doi.org/10.1126/science.1131669.

Boyle, E., 1997. What controls dissolved iron concentrations in the world ocean? Acomment. Mar. Chem. 57, 163–167.

Boyle, E., Lee, J.-M., Echegoyen, Y., Noble, A., Moos, S., Carrasco, G., Zhao, N., Kayser, R., Zhang, J., Gamo, T., Obata, H., Norisuye, K., 2014. Anthropogenic lead emissions in the ocean: the evolving global experiment. Oceanogr. 27, 69–75. https://doi.org/10.5670/oceanog.2014.10.

Boyle, E.A., 1988. Cadmium: chemical tracer of deepwater paleoceanography. Paleoceanography 3, 471–489. https://doi.org/10.1029/PA003i004p00471.

Boyle, E.A., Sclater, F., Edmond, J.M., 1976. On the marine geochemisty of cadmium. Nature 263, 42–44.

Boyle, E.A., Huested, S.S., Grant, B., 1982. The chemical mass balance of the Amazon plume II: copper, nickel and cadmium. Deep. Res. 29, 1355–1364.

Boyle, E.A., Bergquist, B.A., Kayser, R.A., Mahowald, N., 2005. Iron, manganese, and lead at Hawaii Ocean Time-series station ALOHA: temporal variability and an intermediate water hydrothermal plume. Geochim. Cosmochim. Acta 69, 933–952. https://doi.org/10.1016/j.gca.2004.07.034.

Boyle, E.A., John, S., Abouchami, W., Adkins, J.F., Echegoyen-Sanz, Y., Ellwood, M., Flegal, A.R., Fornace, K., Gallon, C., Galer, S., Gault-Ringold, M., Lacan, F., Radic, A., Rehkamper, M., Rouxel, O., Sohrin, Y., Stirling, C., Thompson, C., Vance, D., Xue, Z., Zhao, Y., 2012. GEOTRACES IC1 (BATS) contamination-prone trace element isotopes Cd, Fe, Pb, Zn, Cu, and Mo intercalibration. Limnol. Oceanogr. Methods 10, 653–665. https://doi.org/10.4319/lom.2012.10.653.

Bridgestock, L., van de Flierdt, T., Rehkämper, M., Paul, M., Middag, R., Milne, A., Lohan, M.C., Baker, A.R., Chance, R., Khondoker, R., Strekopytov, S., Humphreys-Williams, E., Achterberg, E.P., Rijkenberg, M.J.A., Gerringa, L.J.A., de Baar, H.J.W., 2016. Return of naturally sourced Pb to Atlantic surface waters. Nat. Commun. 7, 12921.

Bruland, K.W., 1980. Oceanographic distributions of cadmium, zinc, nickel, and copper in the North Pacific. Earth Planet. Sci. Lett. 47, 176–198. https://doi.org/10.1016/0012-821X(80)90035-7.

Bruland, K.W., Lohan, M.C., 2006. Controls of trace metals in eawater. Ocean. Mar. Geochem. 6, 23–47.

Bruland, K.W., Rue, E.L., Smith, G.J., DiTullio, G.R., 2005. Iron, macronutrients and diatom blooms in the Peru upwelling regime: brown and blue waters of Peru. Mar. Chem. 93, 81–103. https://doi.org/10.1016/j.marchem.2004.06.011.

Charette, M.A., Kipp, L.E., Jensen, L.T., Dabrowski, J.S., 2020. The transpolar drift as a source of riverine and shelf - derived trace elements to the Central Arctic Ocean. J. Geophys. Res. Ocean. 1–34 https://doi.org/10.1029/2019JC015920.

Chen, C.-T.A., 1996. The Kuroshio Intermediate water is the major source of nutrients on the East China Sea continental shelf. Oceanol. Acta 19 (5), 523–527.

Chen, C.-T.A., Andreev, A.A., Kim, K.-R., Yamamoto, M., 2004. Roles of continental shelves and marginal seas in the biogeochemical cycles of the North Pacific Ocean. J. Oceanogr. 60, 17–44. https://doi.org/10.1023/B:JOCE.0000038316.56018.d4.

Ciscato, E.R., Bontognali, T.R.R., Vance, D., 2018. Nickel and its isotopes in organic-rich sediments: implications for oceanic budgets and a potential record of ancient seawater. Earth Planet. Sci. Lett. 494, 239–250. https://doi.org/10.1016/j.epsl.2018.04.061.

Comans, R.N.J., van Dijk, C.P.J., 1988. Role of complexation processes in cadmium mobilization during estuarine mixing. Nature 336, 151–154. https://doi.org/10.1038/336151a0.

Cuvelier, M.L., Allen, A.E., Monier, A., McCrow, J.P., Messie, M., Tringe, S.G., Woyke, T., Welsh, R.M., Ishoey, T., Lee, J.-H., Binder, B.J., DuPont, C.L., Latasa, M., Guigand, C., Buck, K.R., Hilton, J., Thiagarajan, M., Caler, E., Read, B., Lasken, R.S., Chavez, F.P., Worden, A.Z., 2010. Targeted metagenomics and ecology of globally important uncultured eukaryotic phytoplankton. Proc. Natl. Acad. Sci. 107, 14679–14684. https://doi.org/10.1073/pnas.1001665107.

Dong, L.X., Guan, W.B., Chen, Q., Li, X.H., Liu, X.H., Zeng, X.M., 2011. Sediment transport in the Yellow Sea and East China Sea. Estuar. Coast. Shelf Sci. 93, 248–258. https://doi.org/10.1016/j.ecss.2011.04.003.

Echegoyen, Y., Boyle, E.A., Lee, J.-M., Gamo, T., Obata, H., Norisuye, K., 2014. Recent distribution of lead in the Indian Ocean reflects the impact of regional emissions. Proc. Natl. Acad. Sci. U. S. A. 111, 15328–15331. https://doi.org/10.1073/pnas.1417370111.

Edmond, J.M., Spivack, A., Grant, B.C., Ming-Hui, H., Zexiam, Chen, Sung, Chen, Zeng Xiushau, C., 1985. Chemical dynamics of the Changjiang estuary. Cont. Shelf Res. 4, 17–36. https://doi.org/10.1016/0278-4343(85)90019-6.

Elbaz-Poulichet, F., Martin, J.M., Huang, W.W., Zhu, J.X., 1987. Dissolved Cd behaviour in some selected french and chinese estuaries. Consequences on Cd supply to the ocean. Mar. Chem. 22, 125–136. https://doi.org/10.1016/0304-4203(87)90004-1.

Fang, T.H., Li, J.Y., Feng, H.M., Chen, H.Y., 2009. Distribution and contamination of trace metals in surface sediments of the East China Sea. Mar. Environ. Res. 68, 178–187. https://doi.org/10.1016/j.marenvres.2009.06.005.

Fitzsimmons, J.N., Zhang, R., Boyle, E.A., 2013. Dissolved iron in the tropical North Atlantic Ocean. Mar. Chem. 154, 87–99. https://doi.org/10.1016/j.marchem.2013.05.009.

Fu, J., Wang, B., Chen, Y., Ma, Q., 2018. The influence of continental air masses on the aerosols and nutrients deposition over the western North Pacific. Atmos. Environ. 172, 1–11. https://doi.org/10.1016/j.atmosenv.2017.10.041.

Guo, L., Chen, Y., Wang, F., Meng, X., Xu, Z., Zhuang, G., 2014. Effects of Asian dust on the atmospheric input of trace elements to the East China Sea. Mar. Chem. 163, 19–27. https://doi.org/10.1016/j.marchem.2014.04.003.

Hawco, N.J., Yang, S.-C., Foreman, R.K., Funkey, C.P., Dugenne, M., White, A.E., Wilson, S.T., Kelly, R.L., Bian, X., Huang, K.-F., Karl, D.M., John, S.G., 2020. Metal isotope signatures from lava-seawater interaction during the 2018 eruption of Kīlauea. Geochim. Cosmochim. Acta 282, 340–356. https://doi.org/10.1016/j.gca.2020.05.005.

He, Q., Bertness, M.D., Bruno, J.F., Li, B., Chen, G., Coverdale, T.C., Altieri, A.H., Bai, J., Sun, T., Pennings, S.C., Liu, J., Ehrlich, P.R., Cui, B., 2014. Economic development and coastal ecosystem change in China. Sci. Rep. 4, 1–9. https://doi.org/10.1038/srep05995.

Ho, T.-Y., Quigg, A., Finkel, Z.V., Milligan, A.J., Wyman, K., Falkowski, P.G., Morel, F.M. M., 2003. The elemental composition of some marine phytoplankton. J. Phycol. 39, 1145–1159. https://doi.org/10.1111/j.0022-3646.2003.03-090.x.

Hu, H., Jin, Q., Kavan, P., 2014. A study of heavy metal pollution in china: current status. Pollut. Control Pol. Countermeas. 6, 5820–5838. https://doi.org/10.3390/su6095820.

Jensen, L.T., Morton, P., Twining, B.S., Heller, M.I., Hatta, M., Measures, C.I., John, S., Zhang, R., Pinedo-Gonzalez, P., Sherrell, R.M., Fitzsimmons, J.N., 2020. A comparison of marine Fe and Mn cycling: U.S. GEOTRACES GN01 Western Arctic case study. Geochim. Cosmochim. Acta 288, 138–160. https://doi.org/10.1016/j.gca.2020.08.006.

Jiang, S., Zhang, J., Zhang, R., Xue, Y., Zheng, W., 2018. Dissolved Lead in the East China Sea with implications for impacts of marginal seas on the open ocean through cross-shelf exchange. J. Geophys. Res. Ocean. 123, 6004–6018. https://doi.org/10.1029/2018JC013955.

Jiann, K., Wen, L., Gong, G., 2009. Distribution and Behaviors of Cd, Cu, and Ni in the East China Sea Surface Water off the Changjiang Estuary, 20, pp. 433–443. https://doi.org/10.3319/TAO.2008.05.09.01(Oc)1.

John, S.G., Conway, T.M., 2014. A role for scavenging in the marine biogeochemical cycling of zinc and zinc isotopes. Earth Planet. Sci. Lett. 394, 159–167. https://doi.org/10.1016/j.epsl.2014.02.053.

John, S.G., Helgoe, J., Townsend, E., 2018. Biogeochemical cycling of Zn and Cd and their stable isotopes in the Eastern Tropical South Pacific. Mar. Chem. 201, 256–262. https://doi.org/10.1016/j.marchem.2017.06.001.

Johnson, K.S., Gordon, R.M., Coale, K.H., 1997. What controls dissolved iron in the world ocean? Mar. Chem. 57, 137–161.

Kang, J., Choi, M.-S., Jeong, K.-S., Lee, C.-B., 2014. Trace metals (Co, Ni, Cu, Cd, and Pb) in the southern East/Japan Sea. Ocean Sci. J. 49, 47–65. https://doi.org/10.1007/s12601-014-0006-9.

Koshikawa, M.K., Takamatsu, T., Takada, J., Zhu, M., Xu, B., Chen, Z., Murakami, S., Xu, K., Watanabe, M., 2007. Distributions of dissolved and particulate elements in the Yangtze estuary in 1997-2002: background data before the closure of the three Gorges Dam. Estuar. Coast. Shelf Sci. 71, 26–36. https://doi.org/10.1016/j.ecss.2006.08.010.

Lagerström, M.E., Field, M.P., Séguret, M., Fischer, L., Hann, S., Sherrell, R.M., 2013. Automated on-line flow-injection ICP-MS determination of trace metals (Mn, Fe, Co, Ni, Cu and Zn) in open ocean seawater: application to the GEOTRACES program. Mar. Chem. 155, 71–80. https://doi.org/10.1016/j.marchem.2013.06.001.

Lemaitre, N., de Souza, G.F., Archer, C., Wang, R.-M., Planquette, H., Sarthou, G., Vance, D., 2020. Pervasive sources of isotopically light zinc in the North Atlantic Ocean. Earth Planet. Sci. Lett. 539, 116216 https://doi.org/10.1016/j.epsl.2020.116216.

Li, L., Liu, J., Wang, X., Shi, X., 2015. Dissolved trace metal distributions and Cu speciation in the southern Bohai Sea. China. Mar. Chem. 172, 34–45. https://doi.org/10.1016/j.marchem.2015.03.002.

Li, L., Wang, X., Liu, J., Shi, X., 2017. Dissolved trace metal (Cu, Cd, Co, Ni, and Ag) distribution and Cu speciation in the southern Yellow Sea and Bohai Sea, China. J. Geophys. Res. Ocean. 122, 1190–1205. https://doi.org/10.1002/2016JC012500.

Li, Q., Cheng, H., Zhou, T., Lin, C., Guo, S., 2012. The estimated atmospheric lead emissions in China, 1990–2009. Atmos. Environ. 60, 1–8. https://doi.org/10.1016/j.atmosenv.2012.06.025.

Liao, W.-H., Ho, T.-Y., 2018. Particulate trace metal composition and sources in the Kuroshio adjacent to the East China Sea: the importance of aerosol deposition. J. Geophys. Res. Ocean. 123, 6207–6223. https://doi.org/10.1029/2018JC014113.

Liao, W.-H., Takano, S., Tian, H.-A., Chen, H.-Y., Sohrin, Y., Ho, T.-Y., 2021. Zn elemental and isotopic features in sinking particles of the South China Sea: Implications for its sources and sinks. Geochim. Cosmochim. Acta 314, 68–84. https://doi.org/10.1016/j.gca.2021.09.013.

Little, S.H., Vance, D., Walker-brown, C., Landing, W.M., 2014. The oceanic mass balance of copper and zinc isotopes, investigated by analysis of their inputs, and outputs to ferromanganese oxide sediments. Geochim. Cosmochim. Acta 125, 673–693. https://doi.org/10.1016/j.gca.2013.07.046.

Liu, W., Tian, J., Chen, L., Guo, Y., 2017. Temporal and spatial characteristics of lead emissions from the lead-acid battery manufacturing industry in China. Environ. Pollut. 220, 696–703. https://doi.org/10.1016/j.envpol.2016.10.031.

Mackey, K.R.M., Chien, C.-T., Post, A.F., Saito, M.A., Paytan, A., 2015. Rapid and gradual modes of aerosol trace metal dissolution in seawater. Front. Microbiol. 5 https://doi.org/10.3389/fmicb.2014.00794.

Mahowald, N.M., Hamilton, D.S., Mackey, K.R.M., Moore, J.K., Baker, A.R., Scanza, R.A., Zhang, Y., 2018. Aerosol trace metal leaching and impacts on marine microorganisms. Nat. Commun. 9, 2614. https://doi.org/10.1038/s41467-018-04970-7.

Martin, J.H., 1990. Glacial-interglacial CO2 change: the iron hypothesis. Paleoceanography 5, 1–13. https://doi.org/10.1029/PA005i001p00001.

Middag, R., van Heuven, S.M.A.C., Bruland, K.W., de Baar, H.J.W., 2018. The relationship between cadmium and phosphate in the Atlantic Ocean unravelled. Earth Planet. Sci. Lett. 492, 79–88. https://doi.org/10.1016/j.epsl.2018.03.046.

Morel, F.M., Price, N.M., 2003. The biogeochemical cycles of trace metals in the oceans. Science 80, 300, 944 LP – 947.

Nishioka, J., Obata, H., 2017. Dissolved iron distribution in the western and central subarctic Pacific: HNLC water formation and biogeochemical processes. Limnol. Oceanogr. 62, 2004–2022.

Pinedo-Gonzalez, P., Hawco, N.J., Bundy, R.M., Armbrust, E.V., Follows, M.J., Cael, B., White, A.E., Ferrón, S., Karl, D.M., John, S.G., 2020. Anthropogenic Asian aerosols provide Fe to the North Pacific Ocean. Proc. Natl. Acad. Sci. 117, 27862–27868.

Posacka, A.M., Semeniuk, D.M., Whitby, H., van den Berg, C.M.G., Cullen, J.T., Orians, K., Maldonado, M.T., 2017. Dissolved copper (dCu) biogeochemical cycling in the subarctic Northeast Pacific and a call for improving methodologies. Mar. Chem. 196, 47–61. https://doi.org/10.1016/j.marchem.2017.05.007.

Price, N.M., Morel, F.M.M., 1991. Colimitation of phytoplankton growth by nikel and nitrogen. Limnol. Oceanogr. 36, 1071–1077.

Rastogi, N., Sarin, M.M., 2013. Temporal variability in residence time of ambient aerosols using environmental ^{210} Pb. Curr. Sci. 105, 1165–1168.

Ren, J.L., Xuan, J.L., Wang, Z.W., Huang, D., Zhang, J., 2015. Cross-shelf transport of terrestrial Al enhanced by the transition of northeasterly to southwesterly monsoon wind over the East China Sea. J. Geophys. Res. Ocean. 120, 5054–5073.

Roshan, S., Wu, J., 2015. The distribution of dissolved copper in the tropical-subtropical North Atlantic across the GEOTRACES GA03 transect. Mar. Chem. 176, 189–198. https://doi.org/10.1016/j.marchem.2015.09.006.

Siefert, R., 2004. The role of coastal zones in global biogeochemical cycles future applications of Thorium-234 in aquatic ecosystems. EOS Trans. Am. Geophys. Union 85, 8–9.

Sohrin, Y., Urushihara, S., Nakatsuka, S., Kono, T., Higo, E., Minami, T., Norisuye, K., Umetani, S., 2008. Multielemental determination of GEOTRACES key trace metals in seawater by ICPMS after preconcentration using an ethylenediaminetriacetic acid chelating resin. Anal. Chem. 80, 6267–6273. https://doi.org/10.1021/ac800500f.

Stein, A.F., Draxler, R.R., Rolph, G.D., Stunder, B.J.B., Cohen, M.D., Ngan, F., 2015. NOAA's HYSPLIT atmospheric transport and dispersion modeling system. Bull. Am. Meteorol. Soc. 96, 2059–2077. https://doi.org/10.1175/BAMS-D-14-00110.1.

Su, J., Pan, Y., Liang, X., 1994. In: Di, Z., Yuan-Bo, L., Cheng-Kui, Z. (Eds.), Kuroshio Intrusion and Taiwan Warm Current BT - Oceanology of China Seas. Springer, Netherlands, Dordrecht, pp. 59–70. https://doi.org/10.1007/978-94-011-0862-1_7.

Sun, X., Fan, D., Liu, M., Liao, H., Tian, Y., 2019. Persistent impact of human activities on trace metals in the Yangtze River estuary and the East China Sea: evidence from sedimentary records of the last 60 years. Sci. Total Environ. 654, 878–889. https://doi.org/10.1016/j.scitotenv.2018.10.439.

Sunda, W.G., 1989. Trace metal interactions with marine phytoplankton. Biol. Oceanogr. 6, 411–442. https://doi.org/10.1080/01965581.1988.10749543.

Sunda, W.G., 1997. Control of dissolved iron concentrations in the world ocean: a comment. Mar. Chem. 57, 169–172.

Sunda, W.G., Huntsman, S.A., 1995. Iron uptake and growth limitation in oceanic and coastal phytoplankton.Pdf.Pdf. Mar. Chem. 50, 189–206.

Tagliabue, A., Bowie, A.R., Boyd, P.W., Buck, K.N., Johnson, K.S., Saito, M.A., 2017. The integral role of iron in ocean biogeochemistry. Nature 543, 51–59. https://doi.org/10.1038/nature21058.

Vance, D., Little, S.H., de Souza, G.F., Khatiwala, S., Lohan, M.C., Middag, R., 2017. Silicon and zinc biogeochemical cycles coupled through the Southern Ocean. Nat. Geosci. 10, 202–206. https://doi.org/10.1038/ngeo2890.

Vink, S., Boyle, E.A., Measures, C.I., Yuan, J., 2000. Automated high resolution determination of the trace elements iron and aluminium in the surface ocean using a towed fish coupled to flow injection analysis. Deep Res. Part I Oceanogr. Res. Pap. 47, 1141–1156. https://doi.org/10.1016/S0967-0637(99)00074-6.

Wang, D., Zhao, Z., Dai, M., 2014. Tracing the recently increasing anthropogenic Pb inputs into the East China Sea shelf sediments using Pb isotopic analysis. Mar. Pollut. Bull. 79, 333–337. https://doi.org/10.1016/j.marpolbul.2013.11.032.

Wang, S.L., Xu, X.R., Sun, Y.X., Liu, J.L., Li, H. Bin, 2013. Heavy metal pollution in coastal areas of South China: a review. Mar. Pollut. Bull. 76, 7–15. https://doi.org/10.1016/j.marpolbul.2013.08.025.

Wang, X., Zhao, L., Xu, H., Zhang, X., 2018. Spatial and seasonal characteristics of dissolved heavy metals in the surface seawater of the Yellow River estuary. China. Mar. Pollut. Bull. 137, 465–473. https://doi.org/10.1016/j.marpolbul.2018.10.052.

Weber, T., John, S., Tagliabue, A., DeVries, T., 2018. Biological uptake and reversible scavenging of zinc in the global ocean. Science 80, 361, 72 LP – 76. https://doi.org/10.1126/science.aap8532.

Windom, H., Smith, R., Rawlinson, C., Hungspreugs, M., Dharmvanij, S., Wattayakorn, G., 1988. Trace metal transport in a tropical estuary. Mar. Chem. 24, 293–305. https://doi.org/10.1016/0304-4203(88)90037-0.

Wu, T., Wu, H., 2018. Tidal mixing sustains a bottom-trapped river plume and buoyant coastal current on an energetic continental shelf. J. Geophys. Res. Ocean. 123, 8026–8051. https://doi.org/10.1029/2018JC014105.

Yin, S., Feng, C., Li, Y., Yin, L., Shen, Z., 2015. Heavy metal pollution in the surface water of the Yangtze estuary: a 5-year follow-up study. Chemoshpere 138, 718–725.

Zhang, J., 1995. Geochemistry of trace-metals from Chinese River estuary systems - an overview. Estuar. Coast. Shelf Sci. 41, 631–658. https://doi.org/10.1006/ecss.1995.0082.

Zhang, J., Zhu, X., Zhang, R., Ren, J., Wu, Y., Liu, S., Huang, D., 2022. Dissolved Fe in the East China sea under the influences of land sources and the boundary current with implications for global marginal seas. Glob. Biogeochem. Cycles 36, e2021GB006946. https://doi.org/10.1029/2021GB006946.

Zhang, M., Sun, X., Xu, J., 2020. Heavy metal pollution in the East China sea: a review. Mar. Pollut. Bull. 159, 111473 https://doi.org/10.1016/j.marpolbul.2020.111473.

Zhang, R., John, S.G., Zhang, J., Ren, J., Wu, Y., Zhu, Z., Liu, S., Zhu, X., Marsay, C.M., Wenger, F., 2015a. Transport and reaction of iron and iron stable isotopes in glacial meltwaters on Svalbard near Kongsfjorden: from rivers to estuary to ocean. Earth Planet. Sci. Lett. 424, 201–211. https://doi.org/10.1016/j.epsl.2015.05.031.

Zhang, R., Zhu, X., Yang, C., Ye, L., Zhang, G., Ren, J., Wu, Y., Liu, S., Zhang, J., Zhou, M., 2018. Distribution of dissolved iron in the Pearl River (Zhujiang) estuary and the northern continental slope of the South China Sea. Deep Sea Res. Part II Top. Stud. Oceanogr. https://doi.org/10.1016/J.DSR2.2018.12.006.

Zhang, R., Jensen, L.T., Fitzsimmons, J.N., Sherrell, R.M., John, S., 2019. Dissolved cadmium and cadmium stable isotopes in the western Arctic Ocean. Geochim. Cosmochim. Acta 258, 258–273.

Zhang, X., Zhong, T., Liu, L., Ouyang, X., 2015b. Impact of soil heavy metal pollution on food safety in China. PLoS One 10, e0135182.

Zhang, X., Li, Z., Takeuchi, N., Wang, F., Wang, S., You, X., Zhou, P., 2017. Heavy metal-polluted aerosols collected at a rural site, Northwest China. J. Earth Sci. 28, 535–544. https://doi.org/10.1007/s12583-017-0728-6.

Zhang, Y., Li, L., Ren, J., He, H., Zhang, R., Zhao, L., Zhang, J., Zhao, M., 2021. Distribution and influencing factors of dissolved manganese in the Yellow Sea and the East China Sea. Mar. Chem. 234, 104002 https://doi.org/10.1016/j.marchem.2021.104002.

Zhao, F.-J., Ma, Y., Zhu, Y.-G., Tang, Z., McGrath, S.P., 2015b. Soil contamination in china: current status and mitigation strategies. Environ. Sci. Technol. 49, 750–759. https://doi.org/10.1021/es5047099.

Zhao, R., Han, B., Lu, B., Zhang, N., Zhu, L., Bai, Z., 2015a. Element composition and source apportionment of atmospheric aerosols over the China Sea. Atmos. Pollut. Res. 6, 191–201. https://doi.org/10.5094/APR.2015.023.

Zhu, X., Zhang, R., Wu, Y., Zhu, J., Bao, D., Zhang, J., 2018. The remobilization and removal of Fe in estuary—a case study in the Changjiang Estuary, China. J. Geophys. Res. Ocean. 123, 2539–2553. https://doi.org/10.1002/2017JC013671.